Lawrence Berkeley Laboratory
UNIVERSITY OF CALIFORNIA

Materials & Molecular
Research Division

CAVITATIONAL EFFECTS DURING CREEP IN POLYCRYSTALLINE ALUMINA

William Richard Blumenthal
(M.S. thesis)

November 1980

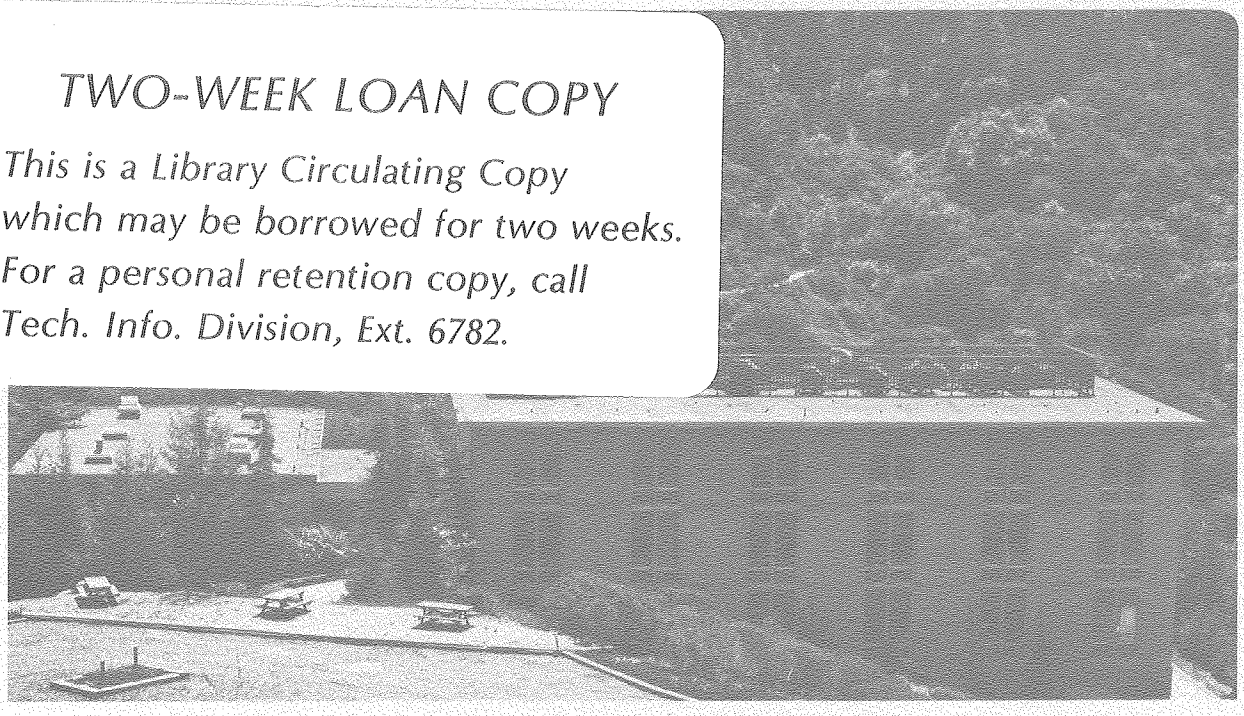

Prepared for the U.S. Department of Energy under Contract W-7405-ENG-48

DISCLAIMER

LBL-11830

CAVITATIONAL EFFECTS DURING CREEP IN POLYCRYSTALLINE ALUMINA

William Richard Blumenthal

M.S. Thesis

November 1980

Lawrence Berkeley Laboratory
University of California
Berkeley, CA 94720

CAVITATIONAL EFFECTS DURING CREEP IN POLYCRYSTALLINE ALUMINA

CONTENTS

CAVITATIONAL EFFECTS DURING CREEP IN POLYCRYSTALLINE ALUMINA

William R. Blumenthal

Materials and Molecular Research Division
Lawrence Berkeley Laboratory
and Department of Materials Science and Mineral Engineering
University of California
Berkeley, CA 94720

ABSTRACT

Cavitation in deformed fine-grained Al_2O_3 was studied as a function of deformation temperature and strain rate. Three distinct cavity profiles were observed in varying proportions depending on the temperature and loading rate. Symmetrically shaped equilibrium cavities were observed at low stress and temperature. Crack-like (non-equilibrium) cavities were observed at higher stress and temperature. Full-facet cavities were observed as the end product of crack-like cavity growth and as a precursor to coalescence. These observations provide strong support for the cavity growth model developed by Chuang, et al. and establish cavitation as an important deformation and failure mechanism in ceramic materials.

I. INTRODUCTION

The advantages of ceramic materials over metallic alloys for severe temperature applications have long been recognized. However, the mechanical properties and modes of failure have not been sufficiently characterized over the range of conditions pertinent to many practical situations.

At low temperature (below about one half the absolute melting temperature) the tensile strength of a ceramic usually coincides with the stress necessary to propagate inherent flaws, usually introduced during machining or processing.[1] The behavior prior to facture is elastic at normal loading rates. However, inelastic behavior can initiate at higher temperatures. Then, since the five independent slip systems necessary for general dislocation deformation are not available in typical polycrystalline ceramics, the plastic deformation behavior is dominated by diffusional processes. A transition in fracture behavior is generally associated with the onset of such diffusional deformation. An understanding of this deformation behavior is a prerequisite for predicting high temperature failure. Observations of high temperature failure stresses much lower than the stress required to extend inherent flaws imply a transition in failure mode from small inherent flaws to larger flaws produced during plastic deformation.[1]

Grain boundary cavities, which develop under the influence of tensile stress, have been identified as the probable source of failure in both metals and ceramics at elevated temperature.[1-3] However,

the cavitation phenomenon has yet to be fully understood at both the atomistic and macroscopic levels.

Greenwood[2] considered four stages of failure due to cavitation; nucleation, growth, coalescence, and rapid fracture. The final stage of rapid fracture can generally be treated with known fracture mechanics methods.

Several cavity nucleation mechanisms have been proposed.[2,4-6] Cavities may open at grain boundary ledges and grain triple points due to local stress concentrations. High stress concentrations can be produced dynamically if the relaxation associated with grain boundary sliding (GBS) is rapid compared with diffusional stress relaxation.[4,5] Condensation of stress-directed vacancies in regions of high tensile stress along grain boundaries is a nucleation mechanism which requires grain boundary diffusion.[2,6] Finally, the decohesion of inclusions is a nucleation mechanism primarily occurring in two phase alloys.[7,8] Boettner and Robertson[9] demonstrated that heterogeneous cavity nucleation developed in copper at the very first stage of creep and continued to occur with further deformation. Greenwood[10] has also shown that a large amount of data were in agreement with a model in which the number of cavities depends linearly on the creep strain (a threshold strain prior to nucleation was also identified). This evidence points out a major difficulty in the study of cavity growth as an individual process since the cavity density does not remain constant as deformation procedes (a common assumption in many growth models).[3,11]

Cavity growth has been proposed to occur by diffusive vacancy coalescence or grain boundary sliding (GBS).[2,12,13] Lack of conclusive evidence over a wide range of conditions leads to the possibility that both mechanisms may occur and dominate cavity growth depending on the given conditions. One of the main problems has been to determine the extent to which diffusive processes contribute to cavity growth vis-a-vis the overall plastic deformation.[2]

This paper describes an attempt to examine diffusive cavitation of macroscopically deformed fully dense ultra-fine grained (1-2 μm) alumina; a study which emphasizes the evolution of cavities at grain boundaries.

Folweiler[14] initially reported the deformation behavior of polycrystalline alumina with a controlled microstructure (7-34 μm). He attempted to demonstrate the effect of grain boundaries on high temperature deformation. He established that the steady-state strain rate exhibited small deviations from stress linearity and was inversely proportional to the square of the average grain size. In addition he observed the appearance of cavities on grain boundaries approximately perpendicular to the applied stress. Variations in grain size, temperature, and strain rate were all observed to influence the appearance of the cavities. However, no correlations were made. The departures from linearity were observed to increase with decreasing grain size, but were not correlated with the dominant variables.

Many researchers[15-18] have since reported the same general behavior for grain sizes from 7 to 100 μm and have concluded that, for this range, the predominant deformation rate is controlled by cation (Al^{+3}) lattice diffusion [the anions (O^{-2}) diffuse very rapidly along the grain boundaries].

More recently Cannon, et al.[19] studied deformation in the range 1-15 μm and generally observed values of the strain rate sensitivity,

$$m \frac{\partial \ln \sigma}{\partial \ln \dot{\varepsilon}} < 1$$

(and as low as 0.6 for the finest grained samples, 1.2 μm). The equivalent grain size exponent was 3 (2.7-2.9). In addition, grain boundary cavitation was detected; but again no correlations were established. It was concluded that, although diffusional creep dominates over the range of temperatures (1200-1750°C) and stresses (1.4-310 MPa) studied, Newtonian-viscous behavior (m = 1) is not always observed. A possible explanation for this non-linear behavior is that grain boundaries do not always act as perfect sources and sinks for vacancies and/or do not always slide easily resulting in "interface-controlled" diffusional creep. Also cited[20] were the possible occurrences of basal slip and non-accommodating GBS. However, Evans[21] has considered these non-diffusive deformation mechanisms and found that they do not contribute significantly to the total creep strain.

Experimental evidence will be presented which shows that grain boundary cavitation contributes significantly to the total applied

strain and that in some cases the diffusive mechanisms controlling cavity growth may be responsible, at least in part, for the observed non-linearity.

II. EXPERIMENTAL

A. Material Characterization

The primary material for the present study was a dense high purity alumina* containing 0.25 percent magnesium oxide (added to enhance densification).

The material was vacuum hot-pressed to nominally theoretical density using graphite dies. The alumina was uniformly black in color indicating that a significant amount of carbon was retained in the material. The average grain size prior to testing was nominally 1-2 μm.

B. Apparatus and Procedures

1. Specimen Preparation

Specimens were cut from the hot-pressed billet to obtain nominal dimensions of 0.03175 m x 0.03175 m x 0.3175 m. The cutting was effected by using a precision diamond saw in order to produce surfaces with close parallelism. Each specimen was then polished on at least one surface using 16,6,1 and finally 0.25 μm diamond abrasive to reduce the influence of surface flaws on the tensile deformation behavior. Specimens that were intended for deformations close to failure strain were given a slight bevel on the corners subject to tensile stresses.

---

*AVCO Corp., Lowell, MA.

2. Experimental Determination of Applied Strain

Ideally a uniaxial tension test would be the simplest and most direct method for measuring the effects of tensile stress on a material. However, severe difficulties arise when attempting to deform ceramic materials in uniaxial tension, due to the lack of satisfactory gripping devices, the extreme temperatures necessary to produce plastic deformation, and the complex and expensive specimen machining required. Hence, it is expedient to perform experiments in flexure. In three point flexure (Fig. 1), the tensile stresses increase from zero at the neutral axis to a maximum along a line on the convex tensile surface, axial with the load.

Because stress and strain vary throughout the specimen it is necessary to choose a reference point for measuring strains and calculating stresses. The point of greatest interest on a specimen is the previously mentioned line of maximum tensile stress at the central convex surface. Direct strain measurements were performed on selected samples by using a series of closely placed lines which were scribed into one of the side surfaces adjacent to the tensile surface (Fig. 2). The scribing was achieved by sliding a Knoop diamond indenter across the surface under a small load. The surface to be scribed was firstly polished to the 0.25 μm diamond abrasive size in order to provide maximum optical contrast for observation and to reduce friction encountered by the indenter.

Next, the specimen was mounted onto a precision micrometer table attached to an Instron* table model testing machine. The Knoop indenter was connected to the Instron cross-head, which was manually operated to control the applied load (as measured by a load cell beneath the micrometer table). A force of approximately 0.25 N was applied and the micrometer table was translated to produce a scribe. A set of scribes were made at a fixed interval of 1.3×10^{-4} m in the central region of the specimen.

Specimens were then deformed at various rates in three point flexure at 1380°C to produce strains of approximately 4, 8 and 11 percent at the central tensile surface.

Using optical microscopy the separation between lines was measured at various points from the tensile surface to the compressive surface and used to calculate values for the plastic strain,

$$\varepsilon = \ln \frac{L_F}{L_0}$$

where L_F is the final separation distance between lines and L_0 is the original interval of 1.3×10^{-4} m.

---

*Instron, Canton, MA.

3. Deformation of Specimens

The mechanical testing apparatus employed to produce deformation was a floor model Instron testing machine with controlled cross-head displacement rates ranging from 8.5×10^{-5} m/sec to 8.57×10^{-8} m/sec.

A 45 N capacity load cell opposite the cross-head was used to measure the load applied to the specimen. A load vs time record was made with an integrated Instron chart recording system. Static load calibration was used for low loading conditions whereas an independently calibrated load cell was employed when high loads were expected. A minimum fullscale deflection of 0.67 N could be achieved with the load cell-strip recording system. Loading was transmitted to the specimen through large-grained creep resistant alumina rams extended into the furnace cavity. The rams were rigidly attached to the cross-head and load cell base with water-cooled fixtures.

A 1600°C maximum temperature air environment furnace employing molybdenum disilicide heating elements was used to control testing temperatures to within ±2°C.

Specimen temperature was measured using a Pt - Pt 10 percent Rh thermocouple placed in direct contact with the sample. The temperature was recorded as a function of time.

Three point flexure was applied to each specimen using a fixture machined from coarse-grained creep-resistant lucalox alumina* such

---

*G.E.

that the lower support span measured 0.025 m. Replaceable 0.0095 m diameter single crystal sapphire rods* were used as the three contacts. Prior to testing, specimens were mounted to the lower fixture supports using an epoxy adhesive in order to maintain proper alignment. The central support piece was then adhered and aligned onto the top of the specimen. An alignment device was used to maintain position while the epoxy cured.

After curing the fixture was placed between the rams inside the room temperature furnace and a small preload corresponding to a maximum tensile stress of approximately 4 MPa was applied. The specimen was then heated to temperature at a rate of between 800°C/hr and 1000°C/hr. At about 500°C the alignment epoxy would vaporize. An automatic heating cycle control was used to maintain only the preload on the specimen during heating. When thermal expansion ceased to increase the load, the preload was removed and the system was allowed to stabilize for a period of 1 hr. All specimens were deformed to a strain of ~0.075 at the central tensile surface. Each specimen was deformed at a different but constantly applied rate. The maximum strain (0.075) was selected to be sufficient for the examination of possible high strain effects. After the prescribed amount of strain had been applied, the specimens were rapidly unloaded in order to measure the resulting anelastic response.

---

*LINDE

4. Post-Deformation Specimen Preparation

After deformation specimens were ground and polished (with 15, 6, 1 and 0.25 μm diamond abrasives) using a high speed polishing machine* on a side adjacent to the tensile surface. The central section of each specimen was cut to fit onto a 10 mm diameter SEM specimen holder using a low speed saw.** The specimens were then ultrasonically cleaned in an acetone bath for 10 min. Thermal etching to reveal the grain boundaries was conducted at 1400°C for 10 to 40 minutes.

5. Microscopy

Scanning electron microscopy was used to examine the polished and etched surface of specimens at magnifications ranging from 500x to 30,000x. The higher magnifications were used to examine typical cavity morphologies. Lower magnifications provided information on the average grain size, the area fraction of void space, and the extent of and variation in cavitation over large areas. Specimens were mounted with silver paint and coated with about 200Å of gold. Typically a 20 kV accelerating potential was employed (10 kV was used occasionally when charging was significant).

C. Experimental Determination of Stress and Strain Rate

Stress and strain rate distributions in three point flexure specimens can not be directly monitored during a deformation test. It is convenient therefore to select a reference location for relating

---

*Pedapin

**Isomet

the measurable quantities of load, deflection rate, and local strain to values of stress and strain rate. The central convex surface, where maximum stress conditions prevail, was chosen for this purpose. Figure 3 shows that a linear relationship between the applied deflection, D, and the locally measured strain, ε, generally exists at this central location, up to strains of at least 0.075. Deviations from linearity only occur at high strains when a high strain rate is applied, due to the presence of cracks initiated on the tensile surface. In the same range, the peak strain rate, $\dot{\hat{\varepsilon}}$, must be linearly related to the displacement rate, $\dot{D}$;

$$\dot{\hat{\varepsilon}} = A\dot{D} \tag{1}$$

where, for the present test geometry, $A = 1.19 \times 10^{-2}\ m^{-1}$. The location of the neutral plane was also determined to be reasonably invarient, at the specimen center, throughout the deformation. the tensile strain, ε, along the central loading axis may thus be written as

$$\varepsilon = \hat{\varepsilon}\,\frac{y}{h} \tag{2}$$

where 2h is the sample height, y is the distance from the neutral axis, and $\hat{\varepsilon}$ is the peak strain at tne surface.

For constant displacement rate conditions the stress, σ, can be readily related to the load, P, under conditions of approximate load invariance. The peak stress, $\hat{\sigma}$, is given by

$$\sigma = \frac{(2n + 1)\ LP}{8\ nb\ h^2} \tag{3}$$

and across the section the stress varies according to

$$\sigma = \frac{y}{h}^{1/n} \frac{(2n + 1)\ LP}{8\ nb\ h^2} = \frac{y}{h}^{1/n} \hat{\sigma} \tag{4}$$

where b is the specimen width, L is the support span, and n is the stress exponent for steady state creep. In general,

$$\dot{\varepsilon} = \sigma^n F(T,S) \tag{5}$$

where T is the temperature, S is the microstructure and F is a function. Combining Eqs. (1), (3) and (5)

$$\log \mathring{D} = n \log P + n \log \frac{(2n + 1)\ L}{8\ nb\ h^2} - \log A + \log [F(T,S)] \tag{6}$$

indicates that, by holding the temperature and microstructure relatively constant, the creep exponent, n, can be directly deduced from the displacement rate and steady state load. Thereafter, the peak stress (coincident with the directly measured peak strain rate) can be deduced from Eq. (3).

III. RESULTS

A. Deformation Behavior

The results will be presented in several forms in order to illustrate the effects of temperature, strain rate, and strain on the deformation behavior of alumina. Firstly, the slope of a log $\hat{P}$ (peak load) vs $\dot{D}$ (displacement rate) plot was used to determine that the value of the stress exponent, n (using Eq. (6)) was ~1.7. Then in Fig. 4 a plot of peak tensile stress vs applied strain rate was constructed for temperatures of 1550, 1650, and 1752 K. Notice that (with the choice of n = 1.7) the slope remains constant over the entire range of imposed strain rates and temperatures.

The apparent activation energy was determined by assuming a constant grain size, to vary from 107 kcal/mole (between 1650 K and 1750 K) to 117 kcal/mole (between 1550 K and 1650 K). The variation in these values will be considered later in terms of trends in grain growth.

Stress vs strain is plotted in Figs. 5-7 for selected strain rates and 1550 K, 1650 K, and 1750 K, respectively. Under the imposition of a constant strain rate, the stress initially increases rapidly as dictated by transient viscous behavior. As deformation continues the stress increases more gradually until steady state viscous behavior is established. This latter behavior can be characterized by a "flow stress," since deformation proceeds at a relatively constant stress (for a given strain rate and temperature).

Many samples exhibited apparent "strain softening" as (or shortly after) the flow state was reached. This is illustrated in Figs. 5-7 where the stress (calculated from the measured load) decays at a relatively constant rate with continued strain. In Fig. 8 the rate of load decay increases with increasing strain rate or with decreasing temperature. However, decay behavior was not observed (at least up to 7-1/2 percent strain) while testing at 1650 k and 1752 K with strain rates less than 1.5×10^{-6} sec^{-1} and 2.5×10^{-5} sec^{-1}, respectively. This behavior will be discussed later in terms of the influence of surface cracks, grain growth, and basal slip.

Linearly plotting flow stress vs strain rate in Fig. 9 fails to reveal the existance of a Bingham type "threshold" stress for plastic deformation.[22] If a strain rate-independent threshold stress exists, then it must be quite small (<3 MPa). Hence, its effect on the deformation behavior would be relatively insignificant.

B. Microstructure

1. Cavitation

All specimens strained to 0.0075 were found to contain voids situated predominantly at the grain boundaries. The small number of intragranual pores present were presumed inherent from processing since the population and distribution of these pores did not appear to be influenced by deformation.

Three particular void shapes were found to occur in varying concentrations depending on the temperature and strain rate. "Equilibrium" cavities (Fig. 10a), characterized by a symmetric

geometry, were observed primarily at grain triple points in samples deformed at slow strain rates (or low stresses) and low temperatures although equilibrium cavities can be observed at all the present testing temperatures if the strain rate (or stress) is sufficiently low. Figure 11a shows an example of equilibrium cavitation in a sample deformed at the slowest strain rate (2.5×10^{-6} sec^{-1}) and highest temperature (1752 K). A distribution of cavity sizes can be observed which implies either continuous nucleation or differential cavity growth. "Non-equilibrium" or "crack-like" cavities (Fig. 10b) are identified by their elongated shape, where the major axis is approximately perpendicular to the applied tensile stress. Crack-like cavities are prevalent at high stress and high temperature, although they have been observed to some degree in all of the present specimens. Figure 11b shows an example of crack-like cavitation. Notice that the maximum cavity width occurs some distance away from the nearest grain junction and that the cavity narrows to a relatively constant width near the tip. The tip of the cavity is presumed to accommodate deformation by moving along the grain boundary until it reaches the next grain junction (while maintaining a dihedral angle of about 90° with respect to the plane of the grain boundary). The third distinct cavity shape is the full-facet cavity (Fig. 10c). Although it is the limiting case of crack-like cavity growth, full-facet cavities will be shown to exhibit deformation behavior distinctly different from crack-like cavities. Figure 12 shows an example of full-facet cavitation in a

specimen tested at a strain rate of 10^{-4} sec^{-1} and at a temperature of 1752 K.

It is interesting to note that only a fraction of the apparently equivalent sites in Figs. 13a and 13b contain observable cavities. This heterogeneous nucleation and growth could be the result of variations in local composition, grain orientation, or grain size. The void area fractions in Figs. 13a and 13b were measured as 3 and 1.5 percent, respectively.

Often full-facet cavities were observed to coalesce, as shown in Fig. 14a. Cavity coalescence undoubtedly influences crack propagation (Fig. 14b) and is therefore a critical mechanism in high temperature failure. Notice that a number of minor cracks have formed, due to cavity coalescence, parallel to the main crack. The main crack is presumed to propagate by linking with the minor cracks.

Examination of the tensile surface of a specimen often revealed the presence of relatively large surface cracks. The surface cracks were as long as 500 μm in highly stressed specimens. Well-developed surface cracks were not observed in specimens tested at 1750 K below a strain rate of 3×10^{-5} sec^{-1} (which corresponds to a flow stress of about 30 MPa). These conditions coincide precisely with those below which flow stress decay is no longer observed.

2. Grain Structure

Lineal analysis[23] of random microstructures after testing revealed that grain growth occurred to some extent in most specimens and that growth was relatively uniform. Table 1 lists the final

average grain size for selected specimens at 1650 K and 1750 K. Specimens tested at 1550 K did not undergo appreciable grain growth from the as-received 1.2 μm average grain size. Since specimens were stabilized at temperature for 1 hr and the subsequent flow stress developed quite rapidly, then the stress exponent previously derived from the peak stress can be considered to be a reasonable estimate. However, the activation energy is quite sensitive to both the grain size and the grain size exponent so that the values previously mentioned may be subject to some error.

IV. DISCUSSION

The most important result of this study has been the observation of diffusive cavitation as a significant deformation and failure mechanism.

Assuming cavitation and diffusional creep to be the only independent deformation mechanisms operating (for simplicity) then,

$$\dot{\epsilon}_{TOT} = \dot{\epsilon}_{CAV} + \dot{\epsilon}_{DIFF\ CREEP} \tag{7}$$

Strain can be produced by both diffusional creep and by cavitation as shown in Fig. 15. The combined thickening of the grain boundary produces strain in the direction of the applied tensile stress. Diffusional creep models have been extensively developed for alumina.[22] For Al_2O_3 the strain rate for diffusional creep is written as

$$\dot{\epsilon} = \frac{14\Omega_c\sigma}{KTd^2} \frac{\left[D_l^{Al} + \frac{\pi\delta D_b^{Al}}{d}\right]\left[D_l^{O} + \frac{\pi\delta D_b^{O}}{d}\right]}{3\left[D_l^{Al} + \frac{\pi\delta D_b^{Al}}{d}\right] + 2\left[D_l^{O} + \frac{\pi\delta D_b^{O}}{d}\right]} \tag{8}$$

which accounts for the diffusion of both aluminum cations and oxygen anions. Of course the present results indicate a non-linear stress dependence which is not predicted by diffusional creep. This implies that the non-linearity may arise from the cavitation component.

Consider the volume, V, of Fig. 15 where a cavity with length, l, is surrounded by boundary area, A. Assuming that the grain boundary

thickening due to cavitation, δ_c, is uniform over the boundary area, then the cavity volume is

$$V_c = A\ \delta_c \tag{9}$$

and the cavitation strain is

$$\varepsilon_c = \frac{\delta_c}{l} = \frac{V_c}{A \cdot l} = \frac{V_c}{V} \tag{10}$$

For a small amount of growth, the grain boundary area can be assumed to remain constant so that

$$\dot{\varepsilon}_c = \frac{d}{dt}\ \frac{V_c}{V} = \frac{\dot{V}}{V} \tag{11}$$

Hence the strain rate produced by cavitation is proportional to the rate of cavity growth for a constant volume.

Recently, Chuang, et al.[11] developed models for "equilibrium" and "non-equilibrium" diffusive cavity growth. Equilibrium growth is defined as the case where surface diffusion is adequate to maintain a symmetric void shape. Hence, growth is limited only by grain boundary diffusion. Non-equilibrium growth implies that insufficient surface diffusion compared to grain boundary diffusion produces voids which are thin and "crack-like." Figure 16 shows typical predictions resulting from Chuang's model assuming an array of pre-existing spherical voids of radius, a, separated by a distance, 2b. The growth

parameter, d, is defined as the ratio of the void diameter to the separation distance, a/b, and represents the extent of cavitation. During the initial stages of cavitation creep, d is very small. Assuming uniform growth, d approaches unity just prior to rupture. The diffusion parameter, Δ, is defined as the ratio of surface to boundary diffusion,

$$\Delta = \frac{D_s \delta_s}{D_b \delta_b} \tag{12}$$

and largely determines the shape of the growing voids. Hence, for a given stress level (defined by the stress parameter, $\sigma b/\gamma_s$) equilibrium cavity growth is favored in the early stages of cavitation (i.e., d is small) or when surface diffusion is relatively rapid (i.e., Δ is large). Conversely, crack-like cavity growth is favored in the latter stages of cavitation (i.e., d is large) or when surface diffusion is slow (i.e., Δ is small). As predicted, a transition in cavity morphology has been observed by varying the stress level at a constant temperature (Figs. 13a and 13b). Observations also indicate that a shape transition occurs by varying the temperature at a constant stress level since the diffusion parameter, Δ, decreases with increasing temperature in Al_2O_3. Hence, full-facet cavities (which are most susceptible to coalescence) are more predominant at higher temperatures for a given stress level. This may partly explain the declining trend in fracture strength with increasing temperature in Al_2O_3.

Again considering bulk deformation, if the rate of cavity growth of individual cavities is assumed constant, then for a given value of strain Greenwood's[2] model of cavity nucleation predicts that the rate of volume change will be directly proportional to the rate of cavity growth. Hence, any non-linearity in the stress dependence of the cavity growth rate will be reflected in the stress dependence of the deformation rate for a given amount of strain.

Advancing Chuang's growth model, Evans[24,29] shows that the growth rate of both equilibrium and full-facet cavities exhibit linear stress-strain rate dependence, whereas only the growth rate of crack-like cavities exhibits second-order stress dependence. Although areal analysis of the void space shows that cavitation can account for as much as 40 percent of the total strain, only a fraction of the cavities (<15 percent) of the cavities are in the crack-like mode. Therefore cavitation can only account for a small part of the non-linearity (~1.2).

An alternate interpretation of the non-linearity involves source-controlled (interface-controlled) diffusional creep as opposed to diffusion-controlled deformation. Diffusion-controlled creep is a mechanism in which the diffusion of vacancies from source to sink controls the rate of deformation. As previously mentioned this mechanism exhibits linear stress-strain rate dependence. On the other hand, a source-controlled mechanism is one in which interface reactions (i.e., source/sink operation) determine the rate of diffusional deformation. Fine-grain materials have been reported[25] to be more

susceptible to source-control. Burton[26] has developed a strain rate equation for source-controlled diffusional creep where spiral dislocations are the grain boundary vacancy sources and sinks,

$$\dot{\varepsilon} = \frac{P_j(z-1)\, b\, D_v \Omega}{8\pi E_d KTd}\, \sigma^2 \qquad (13)$$

where P_j is the probability of finding a jog on a dislocation, Z is the coordination number, b is the Burgers vector, Ω is the vacancy volume, D_v is the vacancy diffusion coefficient, E_d is the energy per unit length of dislocation line, and d is the grain size. In this case, second-order stress dependence is predicted. Burton assumes the fixed spiral dislocations to constantly generate new dislocations at the spiral's center, thereby maintaining a constant dislocation density and creep rate.[27]

Although the intragranular and grain boundary dislocation densities determined from post-deformation TEM studies[20] are low, dislocation motion may still be significant especially at high stress. Figure 17 plots lower yield stress vs strain rate for basal slip in single crystal sapphire[28] superimposed on the polycrystalline flow stress vs strain rate of the present study. The lower basal yield stress is roughly 30 MPa for the temperatures considered and represents the minimum stress required to activate basal slip in favorably oriented grains. Due to the random orientation of grains in a polycrystal, only limited slip is expected to occur. However, Heuer[20] has observed texturing in forged samples of Al_2O_3 which may promote basal slip.

In other words, grains have been observed to rotate with deformation to orientations more favorably to basal slip. Texturing may be enhanced in tensile specimens due to the fewer boundary constraints provided by tensile cavitation. In general, dislocation models of creep predict non-linear stress-strain rate dependencies,[27] however, it is clear that determining the true origin of the observed non-linearity requires further investigation.

The apparent "strain-softening" behavior may be explained by the appearance of well-developed surface cracks only in those specimens exhibiting a decaying flow stress with strain. Invoking stable crack propagation in three point flexure under the imposition of a constant cross-head displacement rate, the decay in the measured load would be due to an increase in the effective compliance as cracks propagate across the specimen. This behavior has been reported by both Warshaw[15] and Coble[16] who observed an apparent increase in the creep rate of statically loaded Al_2O_3 just prior to rupture and associated the increase with the appearance of surface cracks in the samples.

Finally another important observation, especially pertinent to creep rupture prediction, is the inhomogeneous distribution of cavities, particularly at the larger stress levels. Variability in the grain boundary diffusivity is a probable source of this inhomogeneity. Periodic boundaries are likely to exhibit lower diffusivities than most boundaries and, significantly, have not been observed to cavitate.[29] Also boundaries with an excess of impurity species (MgO or SiO_2) in solid solution could exhibit larger diffusivities than

an average boundary. Evans[24] has considered the evolution of inhomogeneous cavity arrays and the subsequent creation of macrocracks.

V. SUMMARY AND CONCLUSION

Cavitation in deformed fine-grained Al_2O_3 was studied as a function of deformation temperature and strain rate. Samples were deformed to 0.075 strain in three-point flexure at 1546, 1646, and 1752 K by imposing strain rates of between 1.25×10^{-6} sec^{-1} and 6.25×10^{-4} sec^{-1}. Strains and strain rates were estimated using local scribe-displacement measurements. A stress exponent was derived from the peak stresses and found to be about 1.7. A phenomenon of flow load decay was observed in a number of samples and was associated with the appearance of surface cracks on the tensile surface.

Diffusive cavitation was considered as an independent deformation mechanism. The rate of cavity growth was shown to be a possible source of stress-strain rate nonlinearity. However, the degree of non-linear cavity growth was not sufficient to produce the observed stress exponent (1.7). Three distinct cavity profiles were observed in varying proportions depending on the temperature and loading conditions. "Equilibrium" cavities were present in all of the samples, but dominated at low stresses and temperatures. They should also dominate during the early stages of creep. Equilibrium cavitation was predicted to exhibit linear stress-strain rate dependence. "Crack-like" cavities were found to be more prevalent at higher stresses and temperatures or during the latter stages of cavitation creep. Second-order stress-strain rate behavior has been predicted for the growth of crack-like cavities. Finally, full-facet cavities were observed as the limiting case of crack-like cavity growth. These cavities appear to be the

precursors to cavity coalescence and ultimately creep rupture, but are predicted to exhibit only linear stress-strain rate growth behavior. Source-controlled (interface-controlled) diffusional creep and dislocation creep were also considered and shown to be possible sources for non-linear stress dependence.

Finally, inhomogeneous cavity evolution and coalescence was observed in all cases which imposes special constraints on cavitation creep rupture models.

In conclusion, these observations provide strong support for the cavity growth model developed by Chuang, et al.[11] and establish cavitation as an important deformation and failure mechanism in ceramic materials.

ACKNOWLEDGEMENTS

I must express my deepest appreciation to all the outstanding people who made this work not only possible, but also rewarding and highly enjoyable. In particular, I thank Professor Anthony G. Evans for his insight, encouragement, and faith; and Professor Joseph A. Pask for his guidance, understanding, and patience. Special thanks must be extended to Nick Burlingame, John Porter, Will Lawrence, and all of the students and staff for their efforts, advice, and most of all, friendship.

This work was supported by the Division of Materials Sciences, Office of Basic Energy Sciences, of the U. S. Department of Energy under contract No. W-7405-ENG-48.

REFERENCES

1. R. W. Davidge and A. G. Evans, Mater. Sci. Engr. 6, 281 (1970).
2. G. W. Greenwood, Fracture 1977, ICF4 1, 293 (1977).
3. D. Hull and D. E. Rimmer, Phil. Mag. 4, 673 (1959).
4. B. J. Nield and A. G. Quarrel, J. Inst. Met. 85, 480 (1956-57).
5. R. C. Gifkins, Fracture, Wiley, NY, 579-627 (1959).
6. R. W. Balluffi and L. L. Seigle, Acta Met. 3, 170 (1955).
7. C. Jenkins, E. Bucknall, and E. Jenkinson, J. Inst. Met. 70, 57 (1944).
8. A. H. Cottrell, Structural Processes in Creep, Iron Steel Inst. and Inst. Met., London, 1-18 (1961).
9. R. C. Boettner and W. d. Robertson, Trans. Met. Soc. AIME 221, 613 (1961).
10. G. W. Greenwood, Phil. Mag. 19, 423 (1969).
11. J. J. Chuang, K. I. Kagawa, J. R. Rice, and L. B. Sills, Acta Met. 27, 265 (1979).
12. R. W. Balluffi and L. L. Seigle, Acta Met. 5, 449 (1957).
13. P. S. Davies and K. R. Williams, Met. Sci. J. 3, 48 (1969).
14. R. C. Folweiler, J. Appl. Phys. 32[5], 773 (1961).
15. S. I. Warshaw and F. H. Norton, J. Am. Ceram. Soc. 45[10], 479 (1962).
16. R. L. Coble and Y. H. Guerard, J. Am. Ceram. Soc. 46, 353 (1963).
17. A. H. Heuer, R. M. Cannon, and N. J. Tighe, Ultrafine-Grain Ceramics, Syracuse Univ. Press, NY, 339-365 (1970).
18. W. R. Cannon and O. D. Sherby, ibid. 60[1-2], 44 (1977).

19. R. M. Cannon, W. H. Rhodes and A. H. Heuer, J. Am. Ceram. Soc. 63[1-2], 46 (1980).

20. A. H. Heuer, N. J. Tighe, and R. M. Cannon, J. Am. Ceram. Soc. 63[1-2], 53 (1980).

21. A. G. Evans, Acta Met. 28, 1155 (1980).

22. R. M. Cannon and R. L. Coble, Deformation of Ceramic Materials, ed., R. C. Bradt and R. E. Jressler, Plenum Press, NY, 61-100 (1975).

23. R. L. Fullman, J. Metals, Trans. AIME 197[3], 447 (1953).

24. A. G. Evans and C. H. Hsueh, to be published.

25. T. H. Alden, Acta Met. 15, 469 (1967).

26. B. Burton, Mat. Sci. Engr. 10, 9 (1972).

27. J. Gittus, Creep, Viscoelasticity and Creep Fracture in Solids, Wiley, NY (1975).

28. M. L. Kronberg, J. Am. Ceram. Soc. 45[6], 274 (1962).

29. J. R. Porter, W. Blumenthal, and A. G. Evans, to be published.

FIGURE CAPTIONS

Fig. 1. Three-point bending fixture used in a constant cross-head speed testing machine with an attached high temperature furnace.

Fig. 2. Load and displacement are measured directly. Local strains are measured by scribe separation.

Fig. 3. Cross-head displacement is linearly related to strain by linear elasticity below 10 percent outer fiber strain.

Fig. 4. The creep behavior of 2 μm Al_2O_3 + 0.25 percent MgO is characterized by a strain rate exponent, m = 0.6, and an activation energy of 480 KJ/mole.

Fig. 5. Tensile stress-strain rate behavior at 1546 K. The flow stress appears to decay after reaching a peak for many strain rates.

Fig. 6. Tensile stress-strain rate behavior at 1646 K.

Fig. 7. Tensile stress-strain rate behavior at 1752 K.

Fig. 8. Strain rate vs load decay rate illustrates that the decay behavior is definitely a function of temperature and strain rate. Apparently the decay behavior disappears with high temperature and slow strain rates indicating a possible brittle to ductile transition.

Fig. 9. Plotting flow stress vs strain rate on a linear scale illustrates the lack of a "threshold" stress.

Fig. 10. (a) Schematic of an equilibrium shaped cavity. Symmetry is maintained when surface diffusion is of the same order as grain boundary diffusion. (b) Schematic of a non-equilibrium or crack-like cavity. Grain boundary diffusion is much greater than surface diffusion such that the cavity tip grows down boundaries perpendicular to the applied tensile stress. (c) Schematic of a full-facet cavity which is the limiting case of crack-like cavity growth. Further growth occurs by surface separation.

Fig. 11. (a) Micrograph of an equilibrium cavity. (b) Micrograph of a crack-like cavity.

Fig. 12. Micrograph of a full-facet cavity.

Fig. 13. (a) Equilibrium cavitation at T = 1752 K and $\dot{\varepsilon} = 2.5 \times 10^{-6}$ s^{-1} with 0.075 strain. (b) Crack-like and full-facet cavitation at T = 1752 K and $\dot{\varepsilon} = 1.2 \times 10^{-4}$ s^{-1} with 0.075 strain.

Fig. 14. (a) Coalescence of full-facet cavities into parallel arrays. (b) Crack propagation due to linking of cavity arrays.

Fig. 15. Diffusional creep and cavitation creep produce strain in the direction of the applied tensile stress by atom diffusion which increases the "effective" grain boundary thickness.

Fig. 16. Recent cavity growth models predict transitions from equilibrium cavity growth to crack-like cavity growth. Preliminary experimental evidence supports these predictions.

Fig. 17. Superimposing single crystal basal slip behavior and polycrystalline creep behavior demonstrates that some basal slip could occur in favorably oriented grains leading to a more compliant material.

TABLE 1: SELECTED* VALUES OF THE AVERAGE FINAL GRAIN SIZE

TEMP (K)	STRAIN RATE (sec^{-1})	TIME AT TEMP (min)**	GRAIN SIZE (μm)
	6.25×10^{-6}	260	2.2
1646	1.25×10^{-5}	160	1.8
	2.50×10^{-5}	110	1.5
	2.50×10^{-6}	560	3.4
	1.25×10^{-5}	160	3.2
1752	6.25×10^{-5}	80	2.8
	1.25×10^{-4}	70	2.0
	2.50×10^{-4}	65	1.9

* SAMPLES TESTED AT 1546 K HAD A GRAIN SIZE OF 1.25 - 1.3 μm.

** VALUES INCLUDE A ONE HOUR STABILIZATION PERIOD.

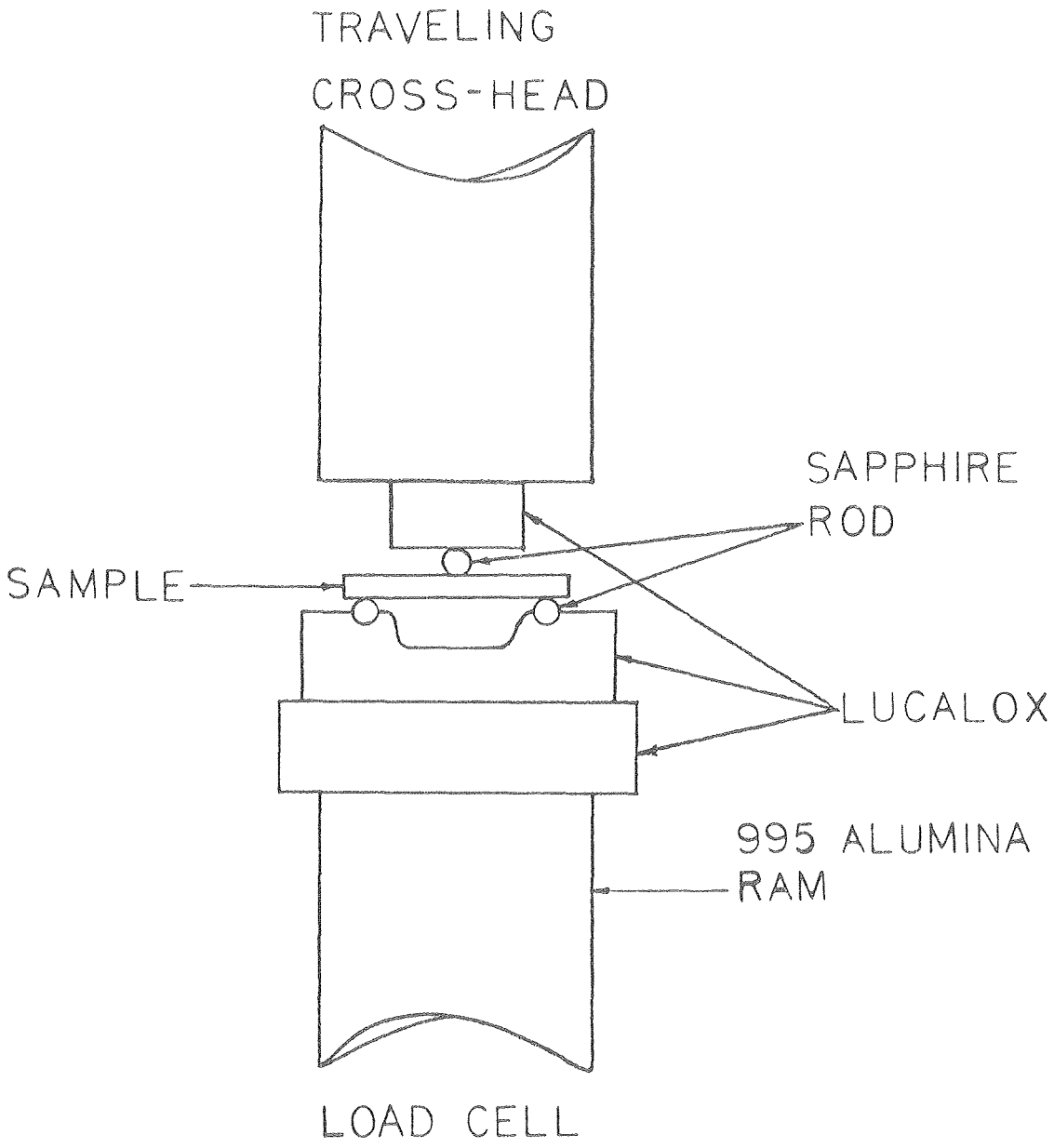

XBL 805-5202

Fig. 1

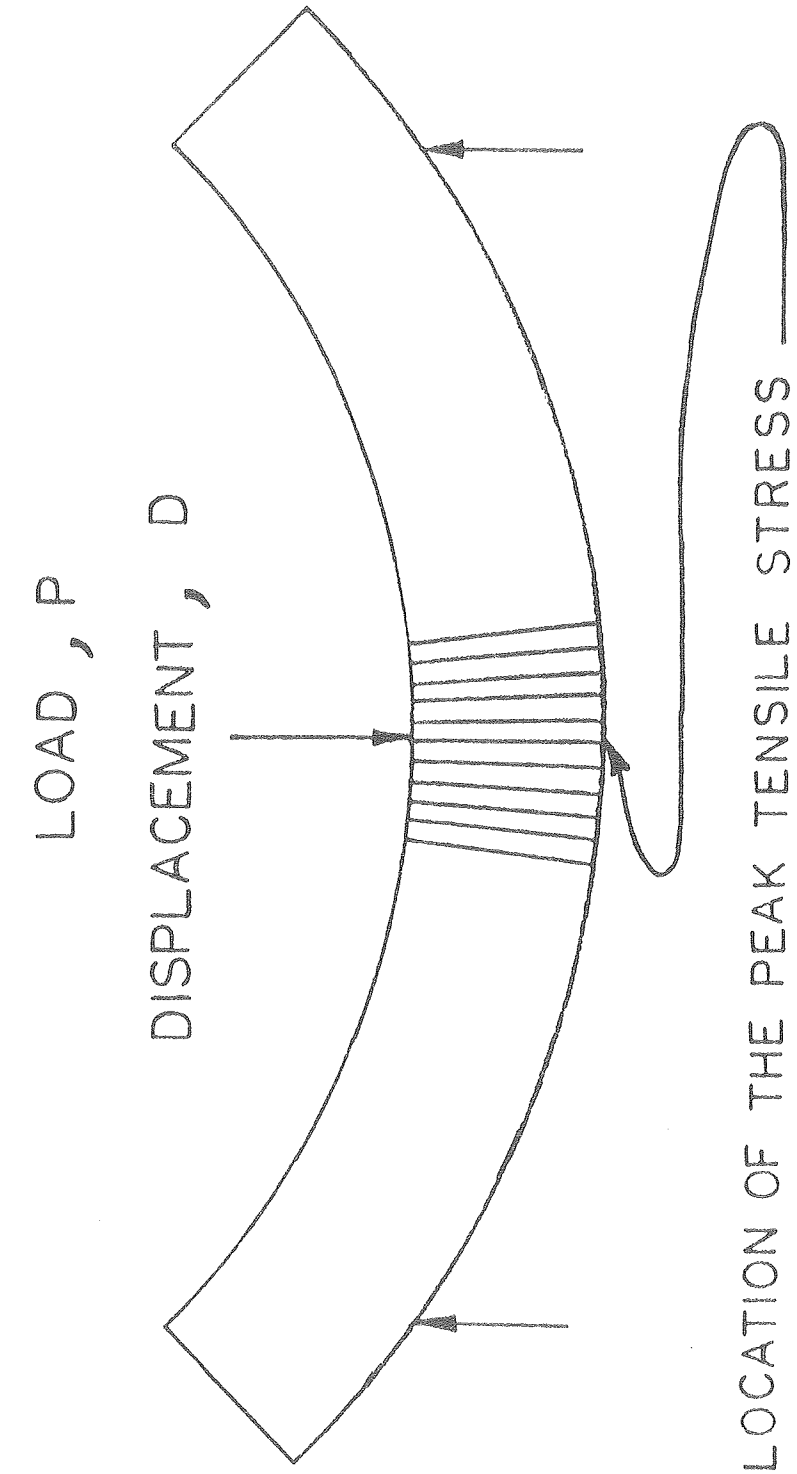

XBL 809-11660

Fig. 2

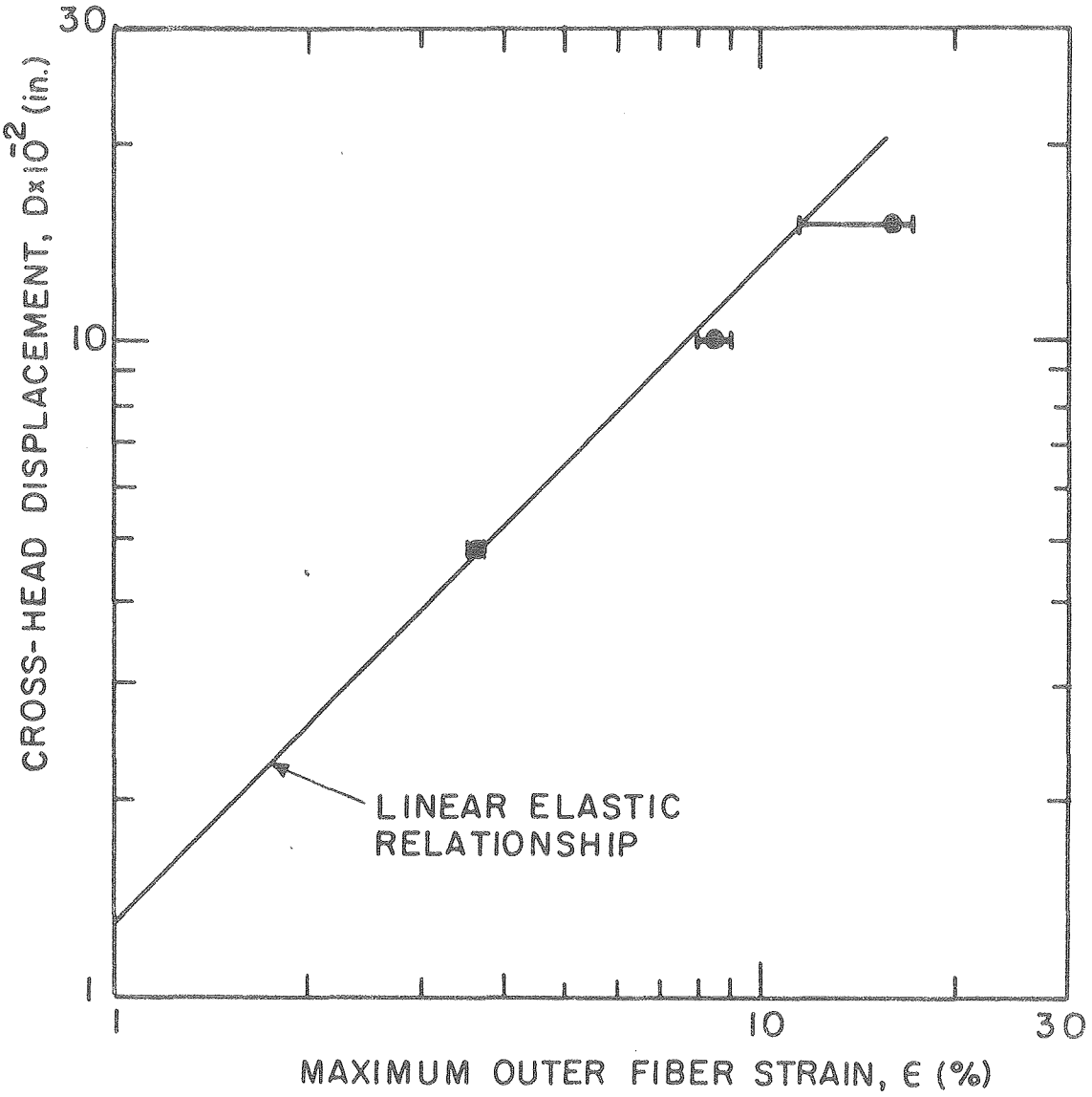
CROSS-HEAD DISPLACEMENT, D x 10^{-2} (in.)
30
10
1
LINEAR ELASTIC
RELATIONSHIP
1
10
30
MAXIMUM OUTER FIBER STRAIN, ε (%)
XBL 805-5201

Fig. 3

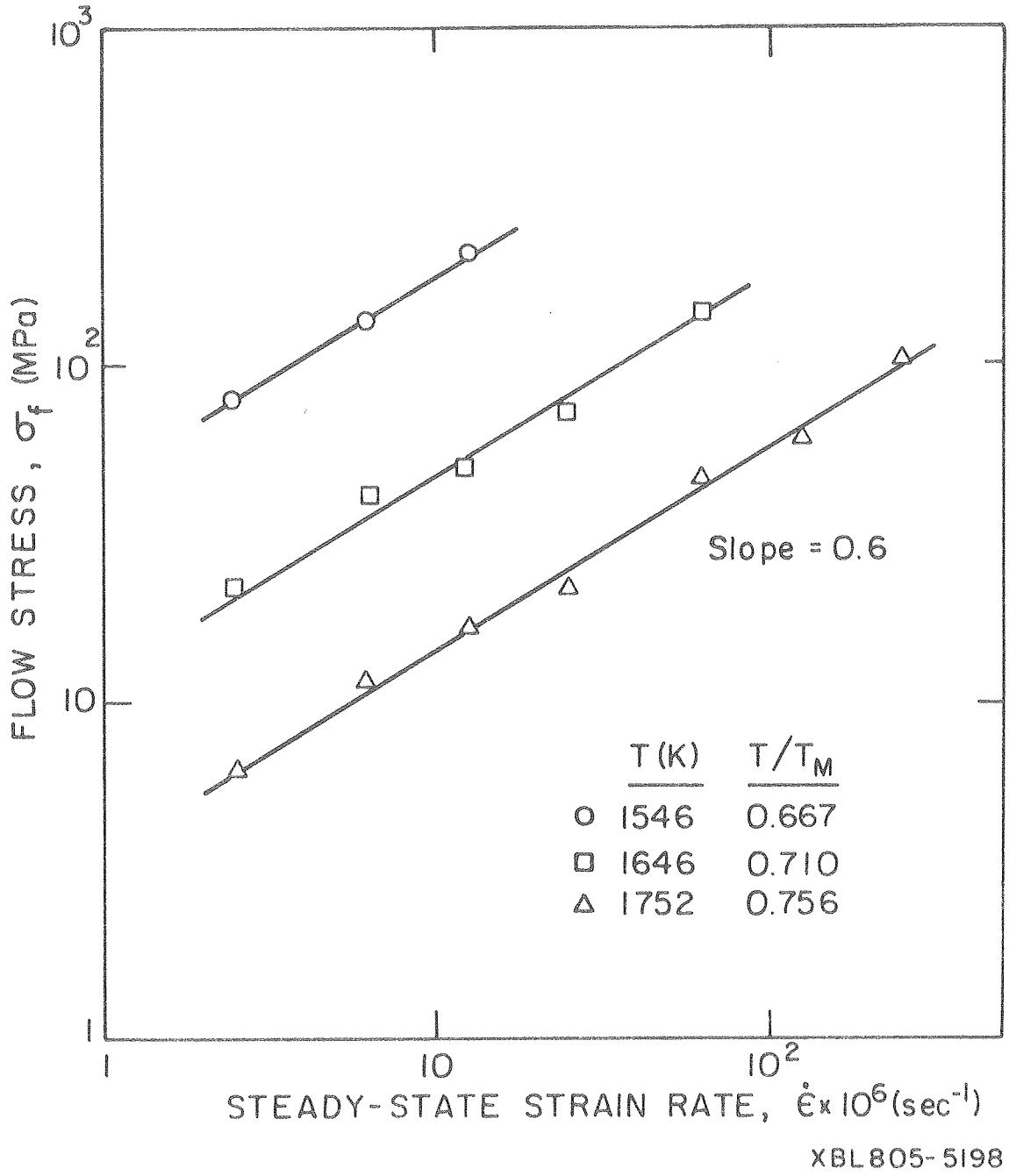
FLOW STRESS, σ_f (MPa)
10^3
10^2
10
1
1
10
10^2
STEADY-STATE STRAIN RATE, $\dot{\epsilon} \times 10^6 (sec^{-1})$
Slope = 0.6
T(K) T/T$_M$
○ 1546 0.667
□ 1646 0.710
△ 1752 0.756
XBL805-5198

Fig. 4

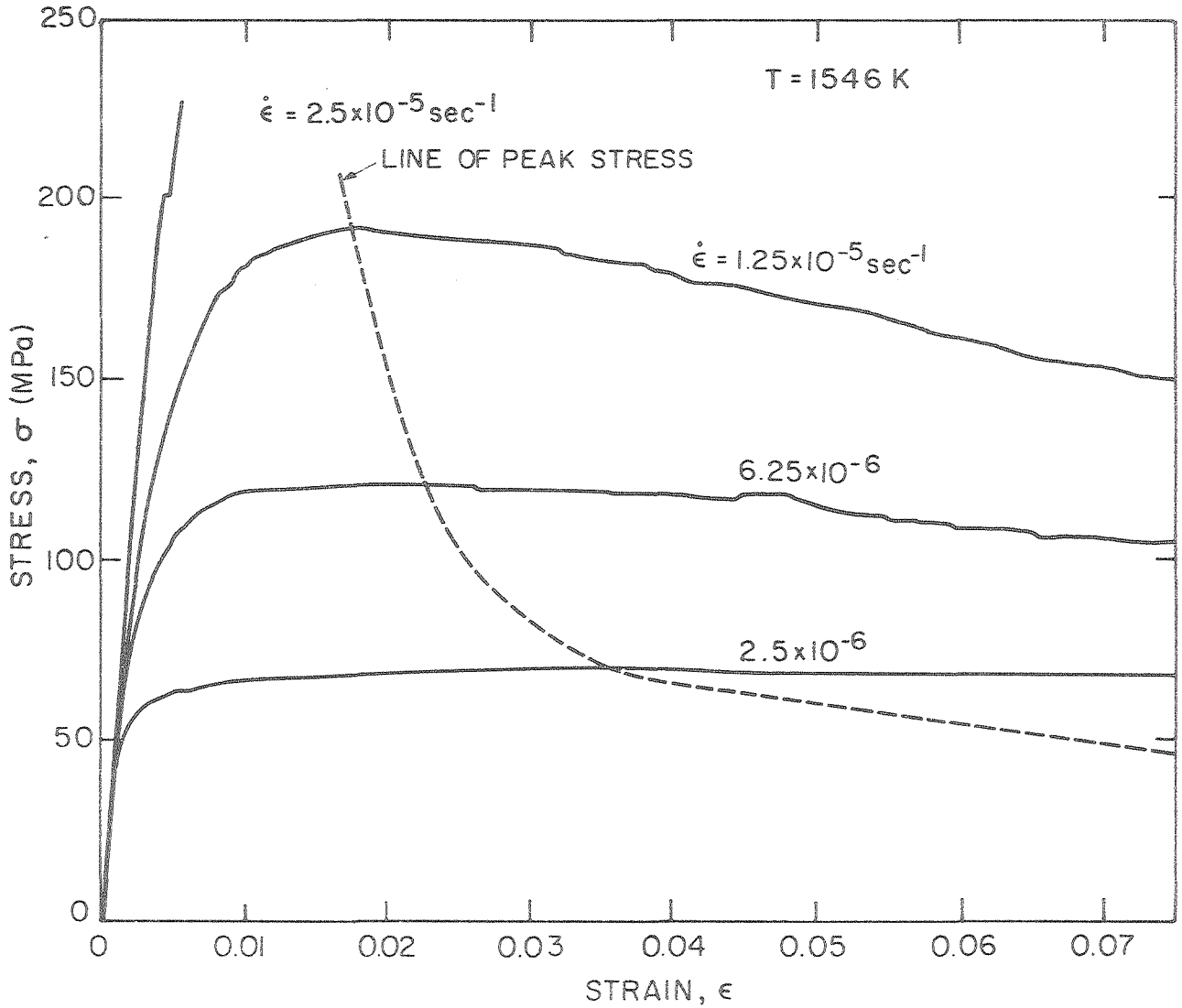

XBL805-5196

Fig. 5

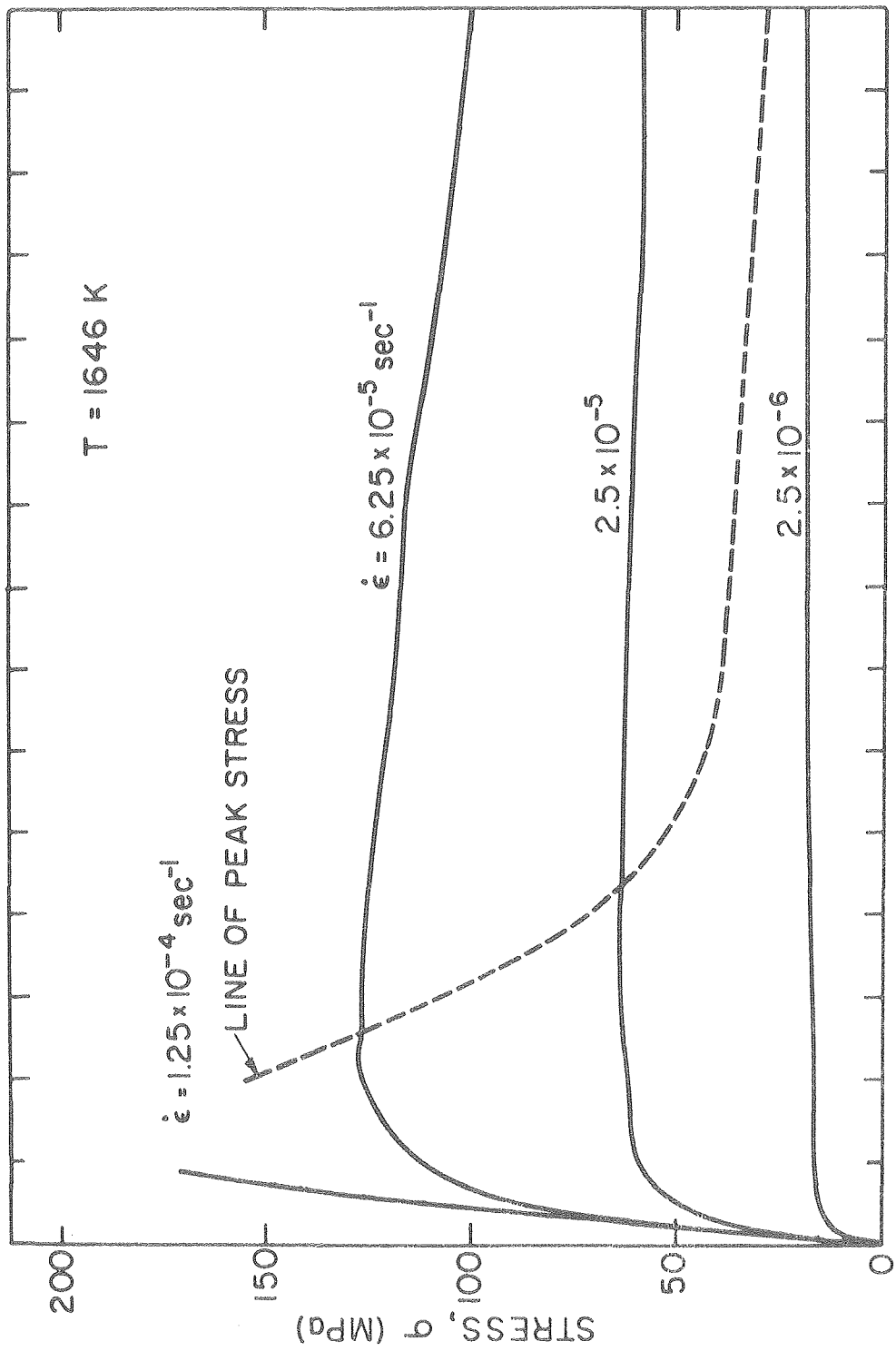

XBL805-5195

Fig. 6

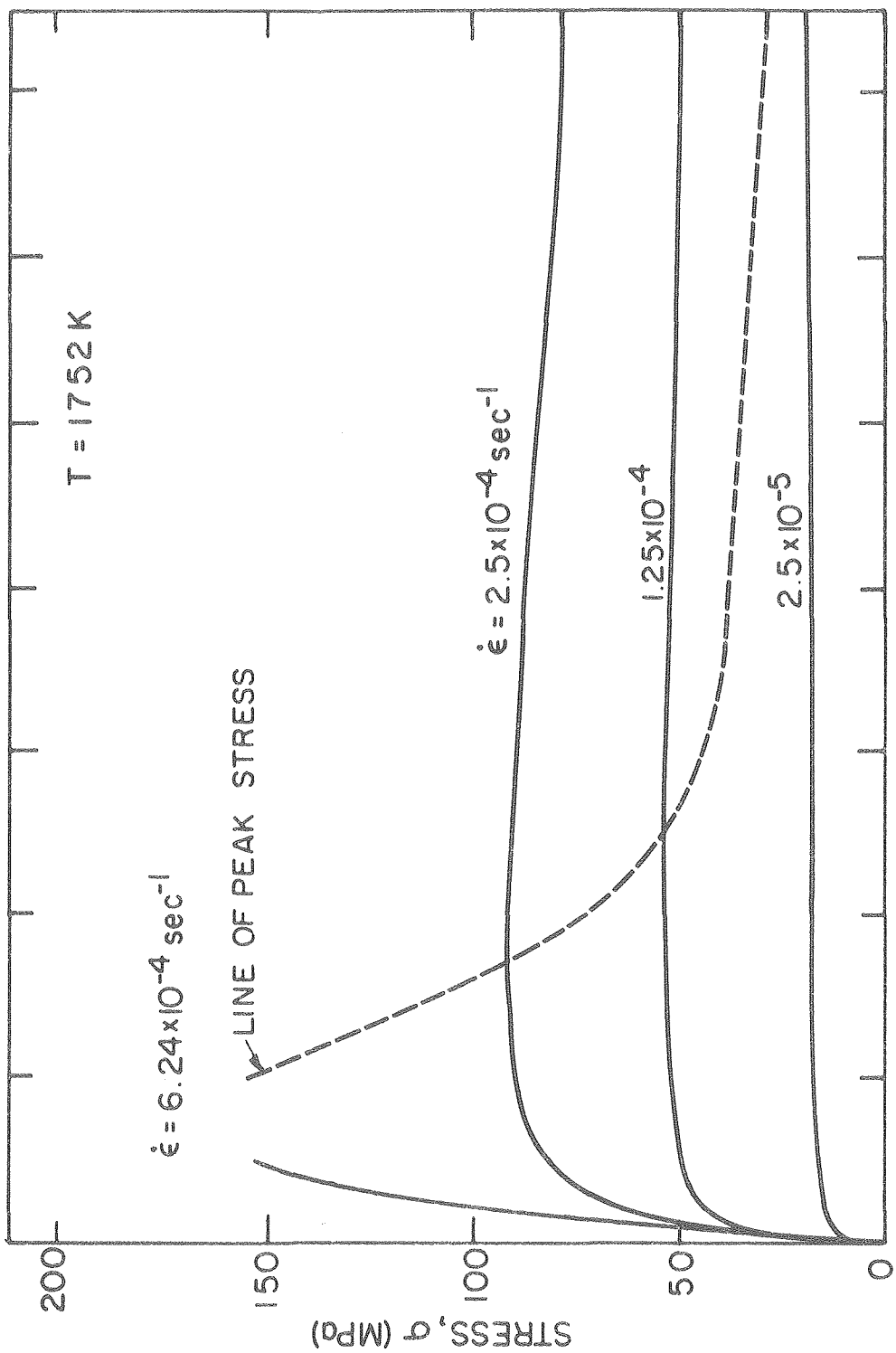

XBL805-5197

Fig. 7

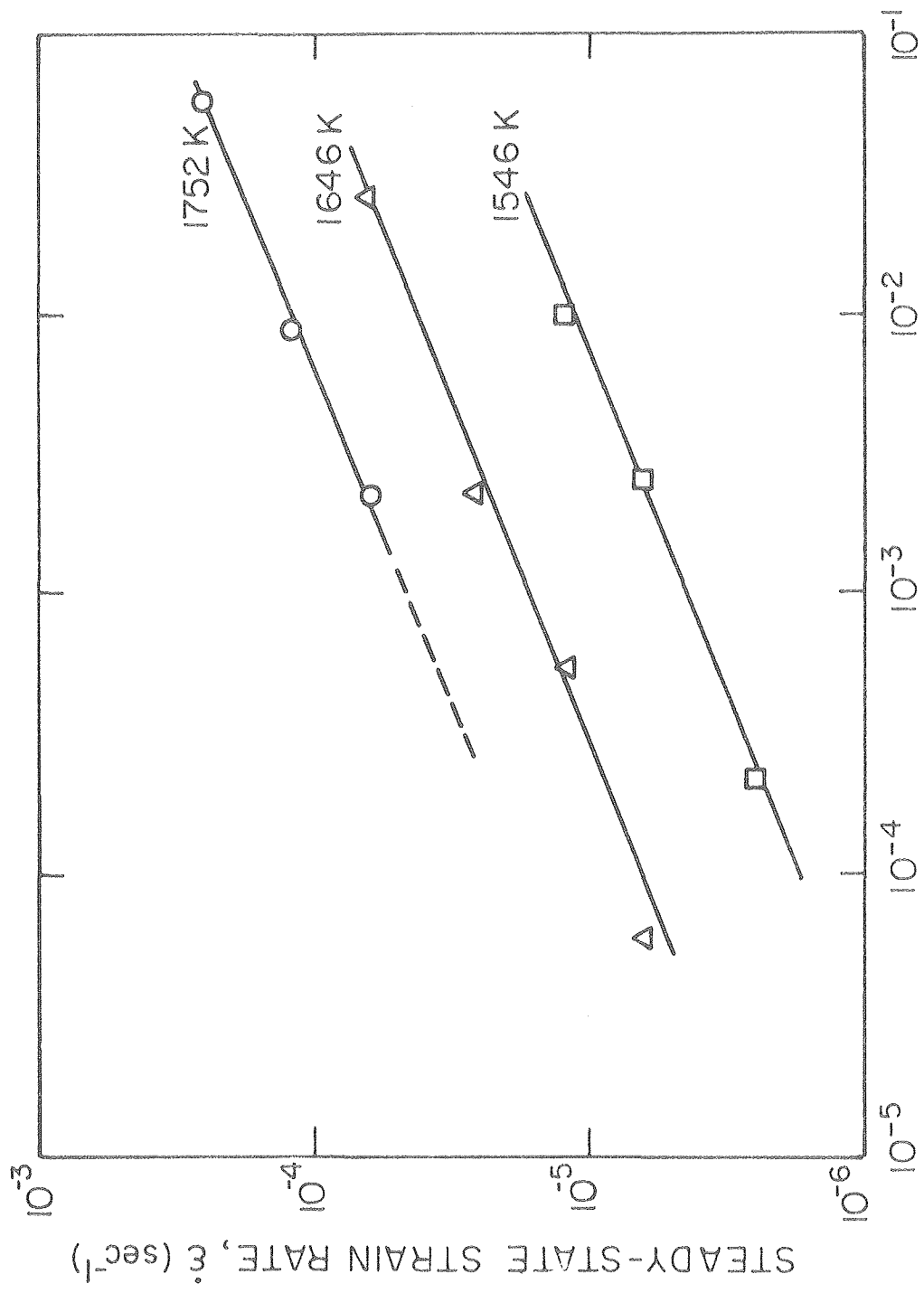

XBL 808-5721

Fig. 8

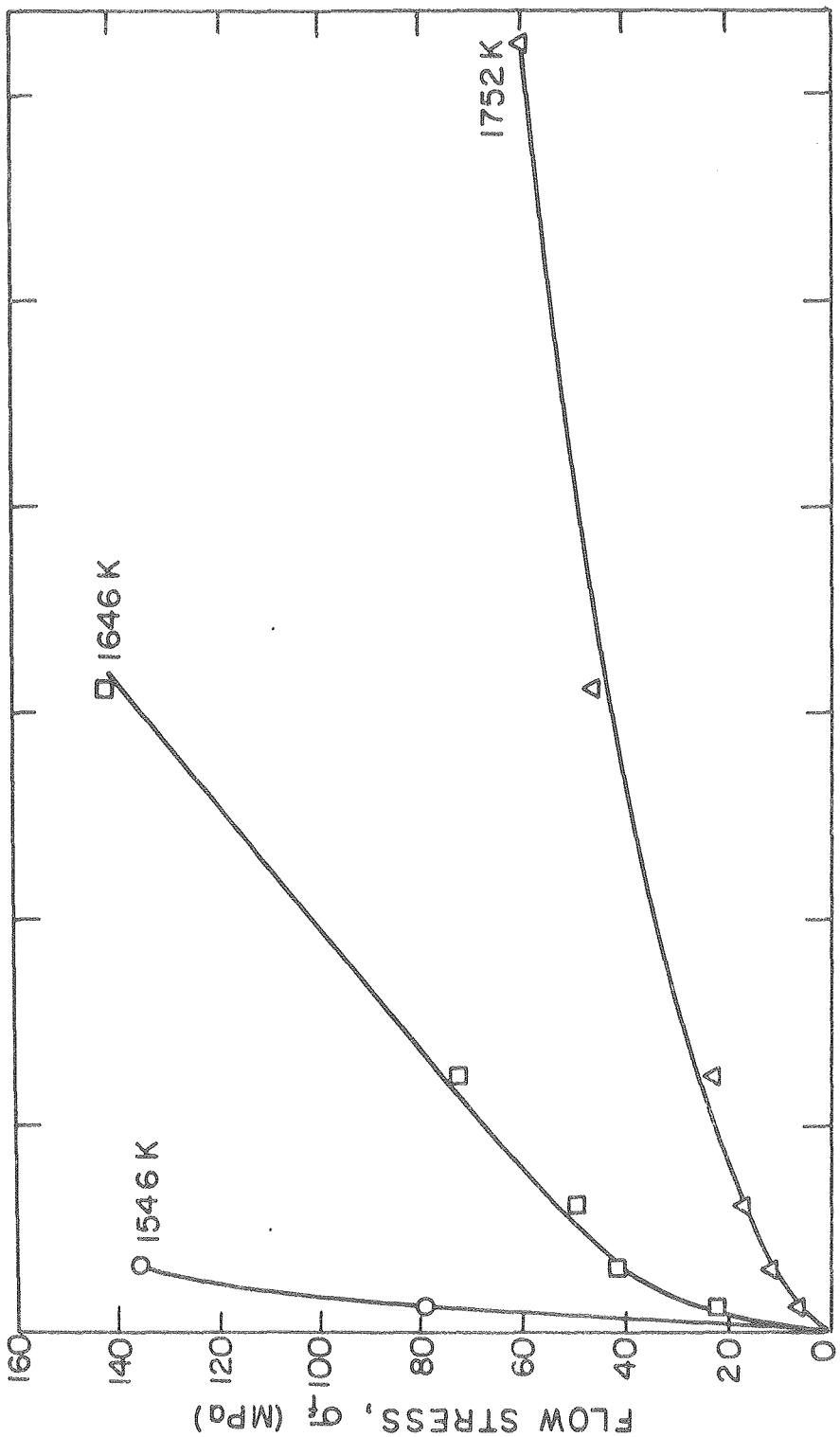

XBL805-5200

Fig. 9

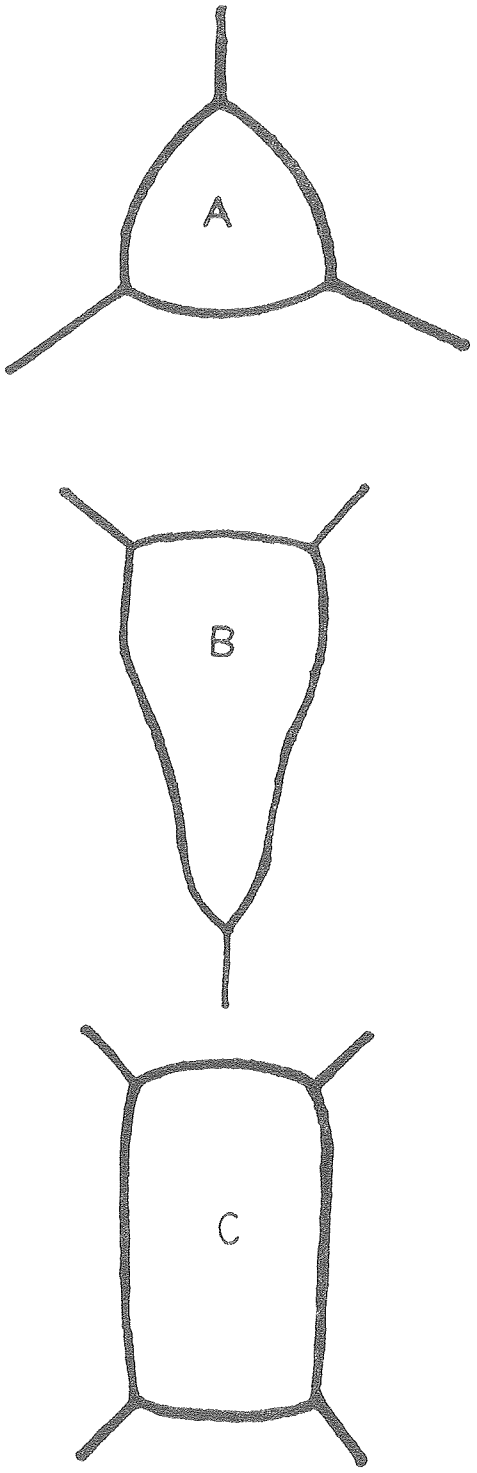

XBL 809-11659

Fig. 10

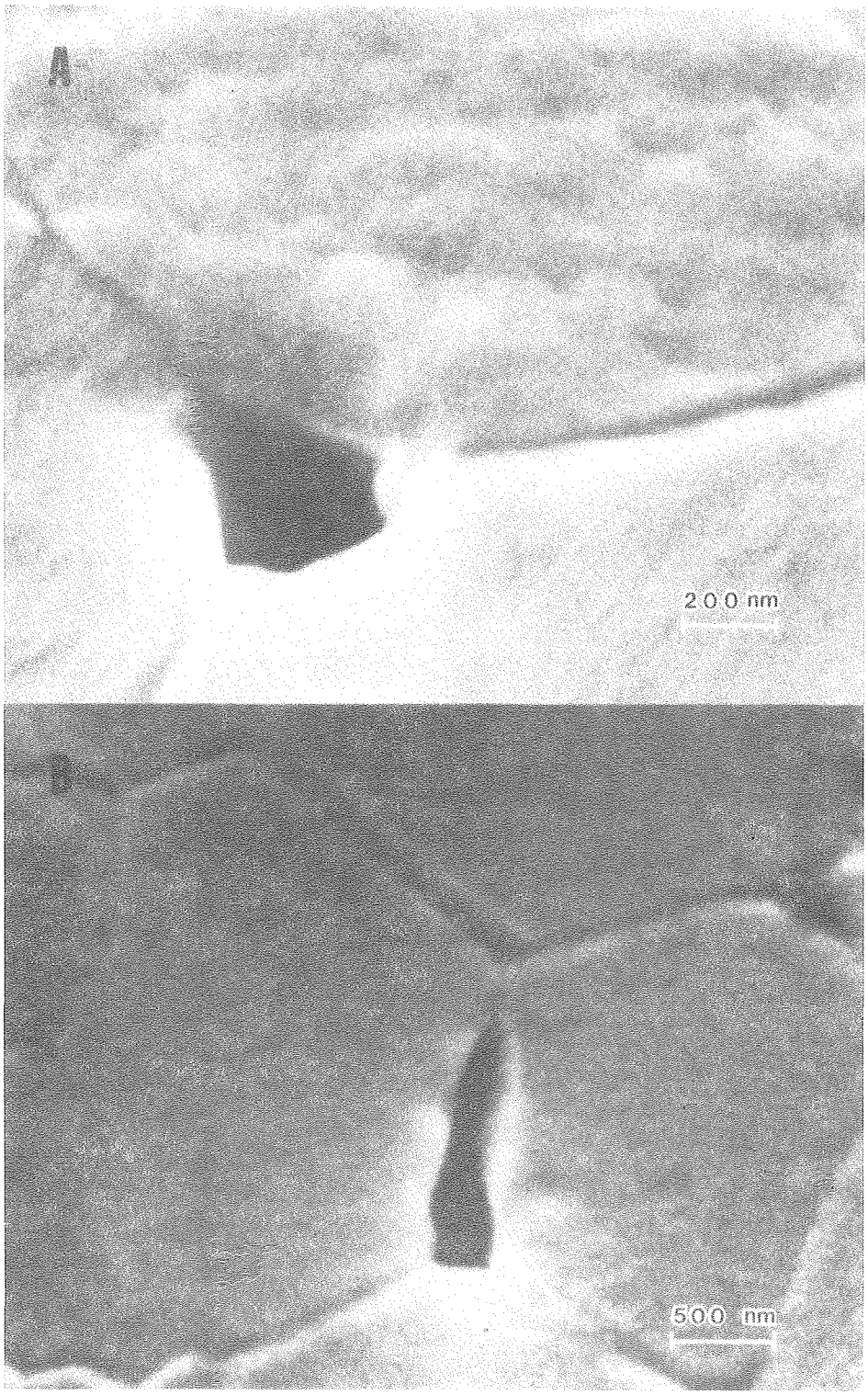

XBB 809-10353

Fig. 11

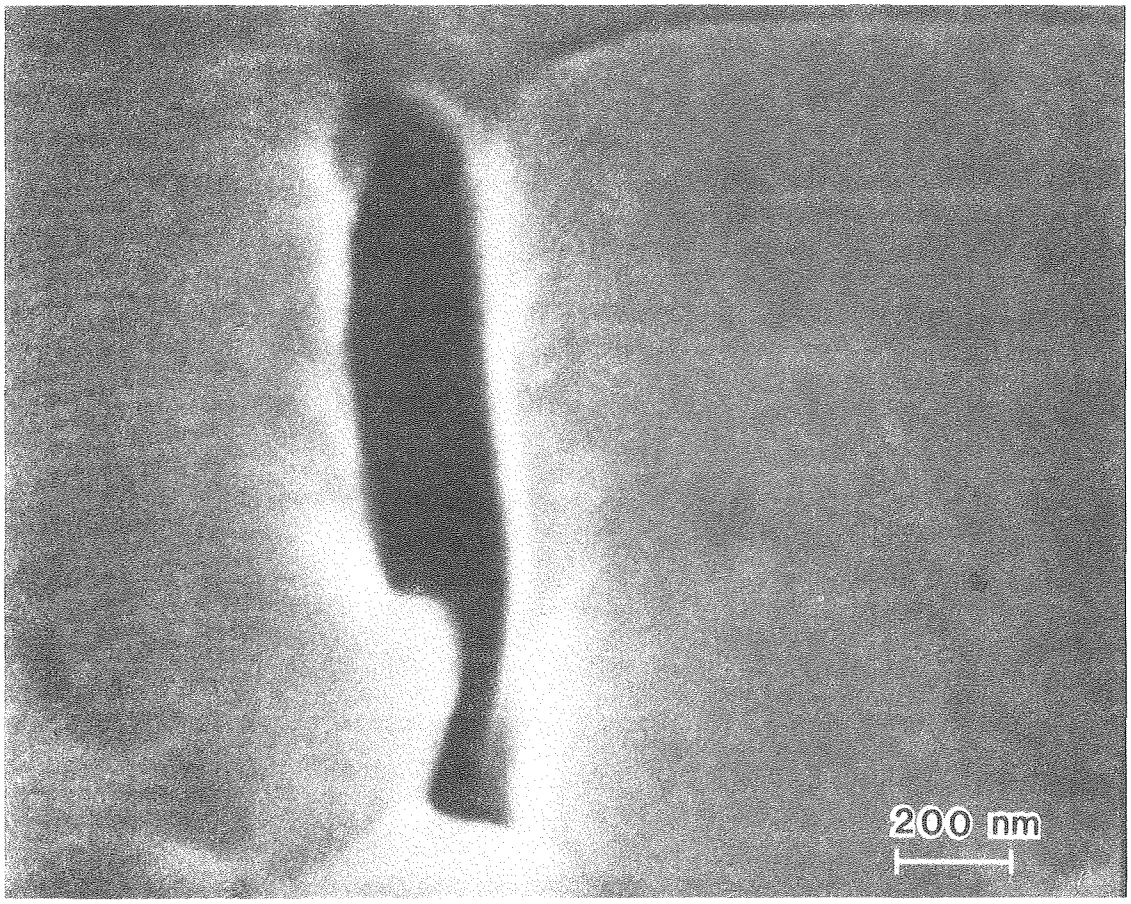

XBB 809-10352

Fig. 12

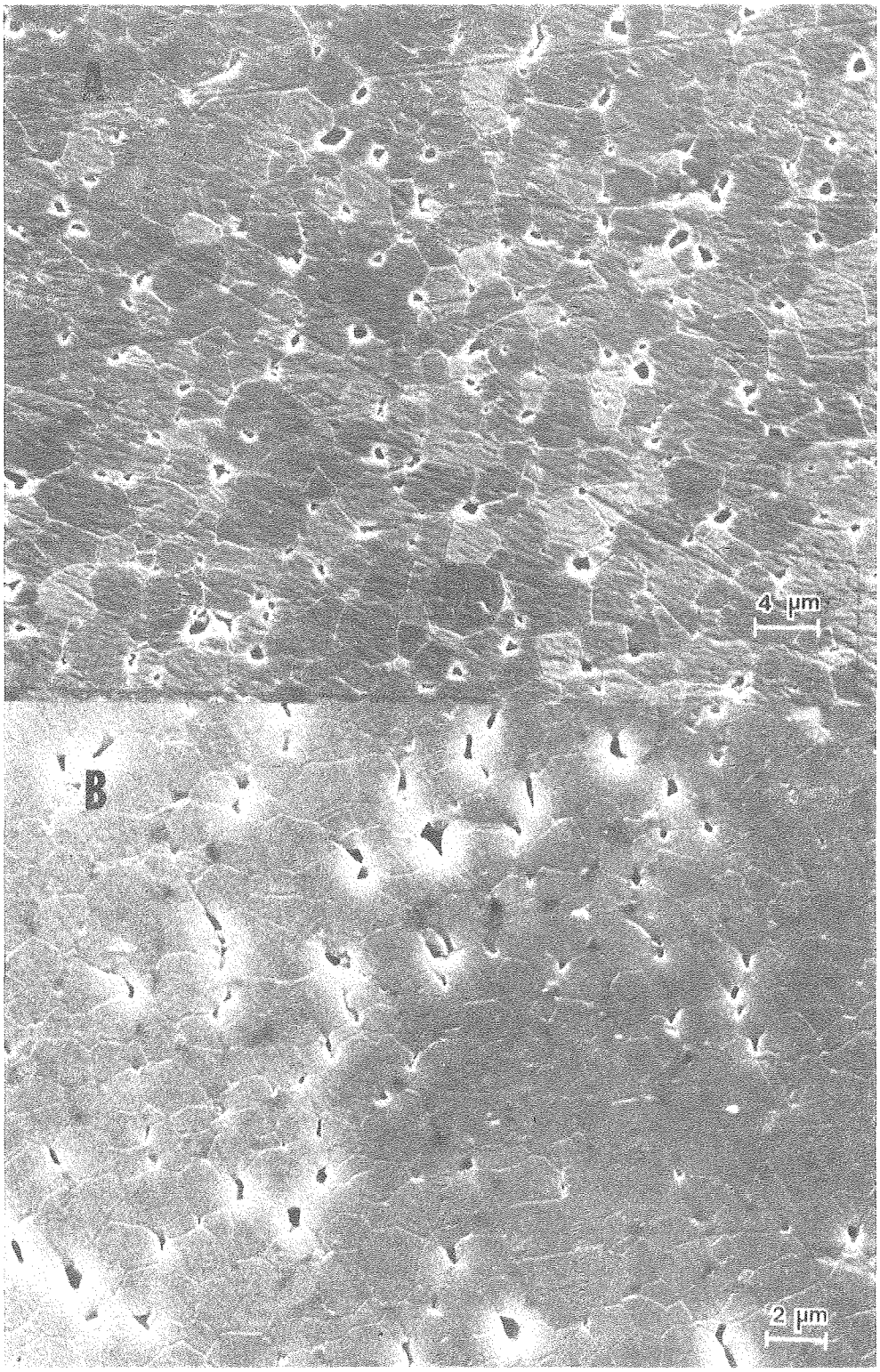

XBB 809-10354

Fig. 13

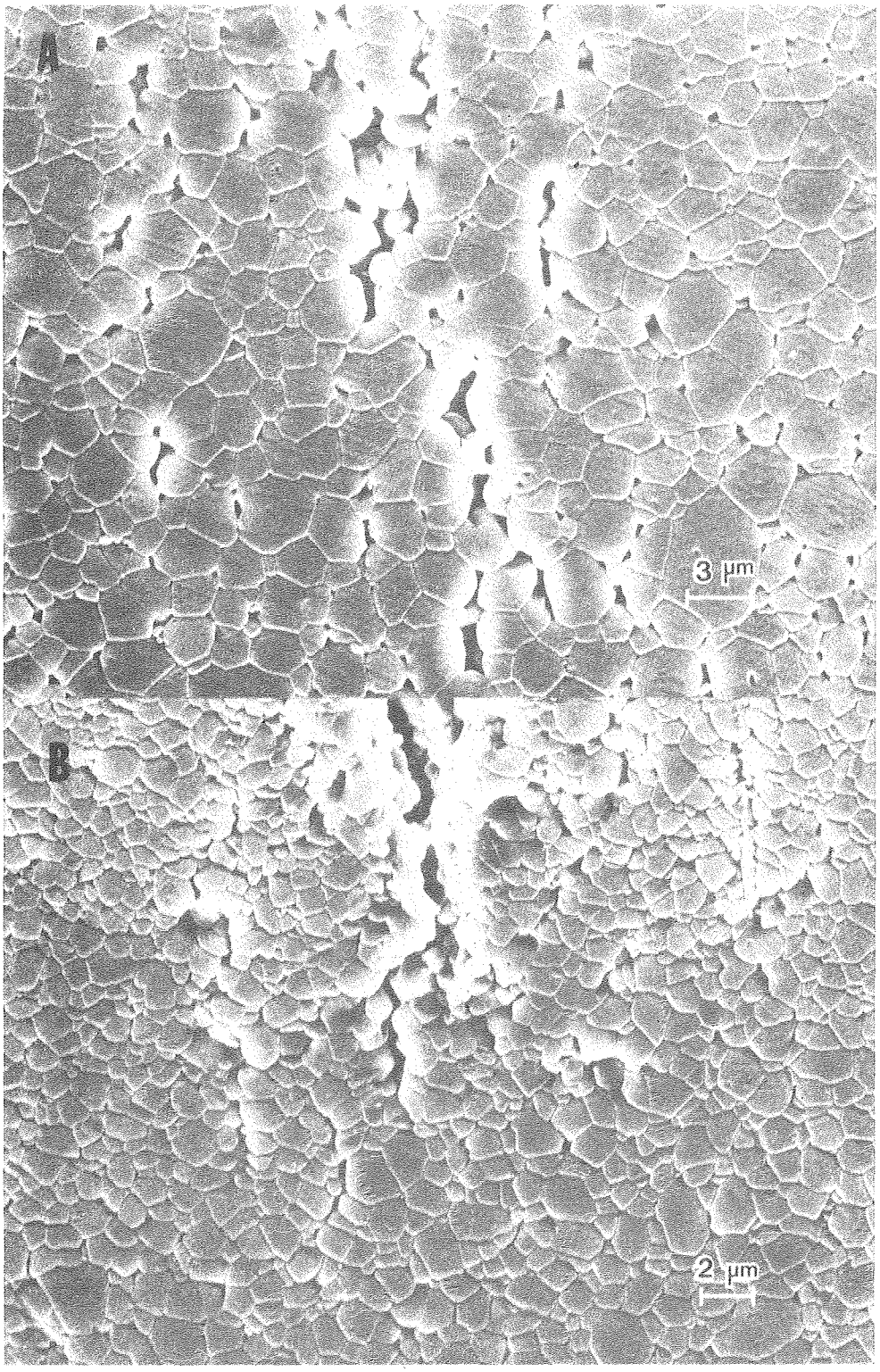

XBB 809-10351

Fig. 14

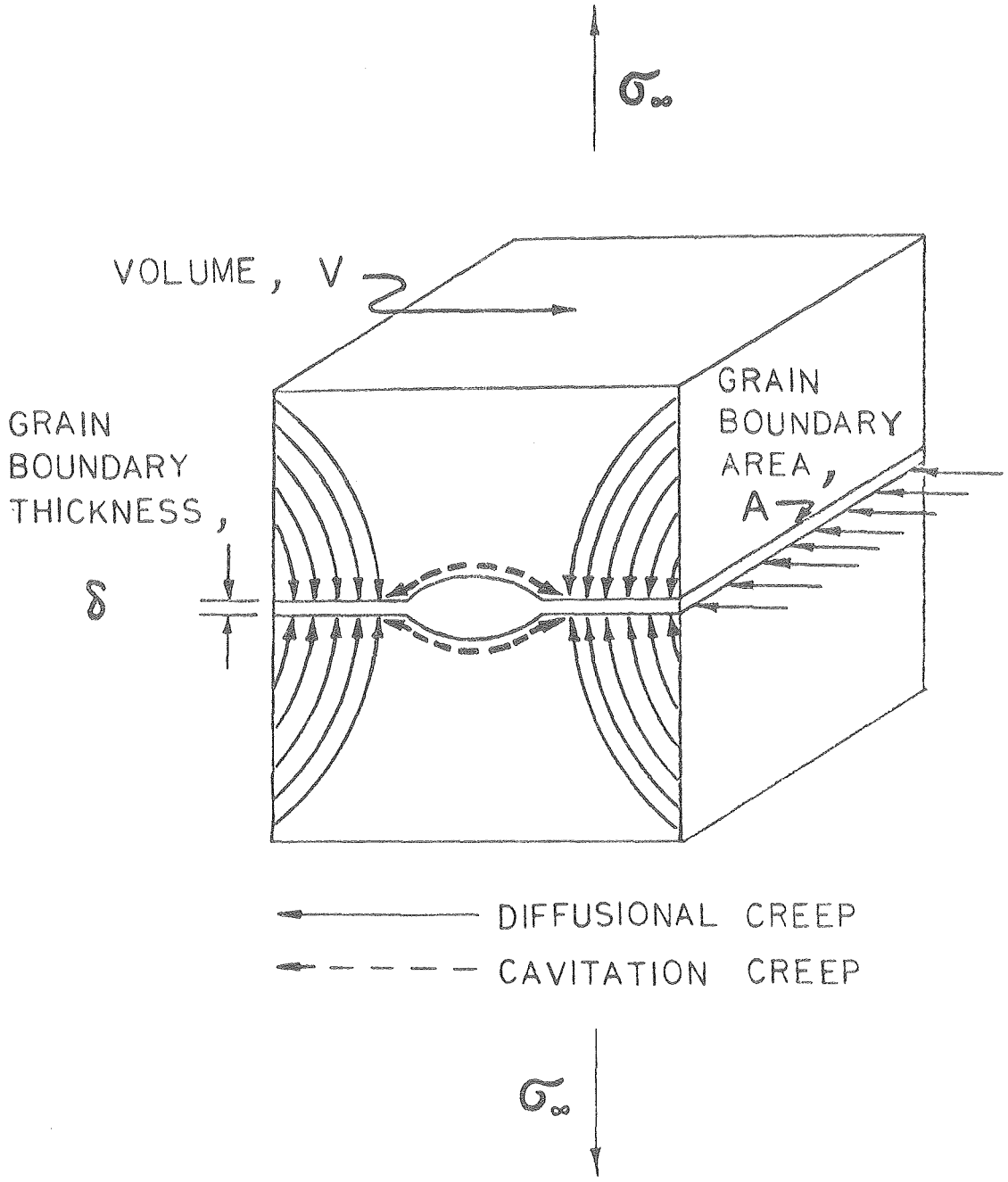
σ_∞
VOLUME, V
GRAIN BOUNDARY THICKNESS, δ
GRAIN BOUNDARY AREA, A
DIFFUSIONAL CREEP
CAVITATION CREEP
σ_∞
XBL 809-11658

Fig. 15

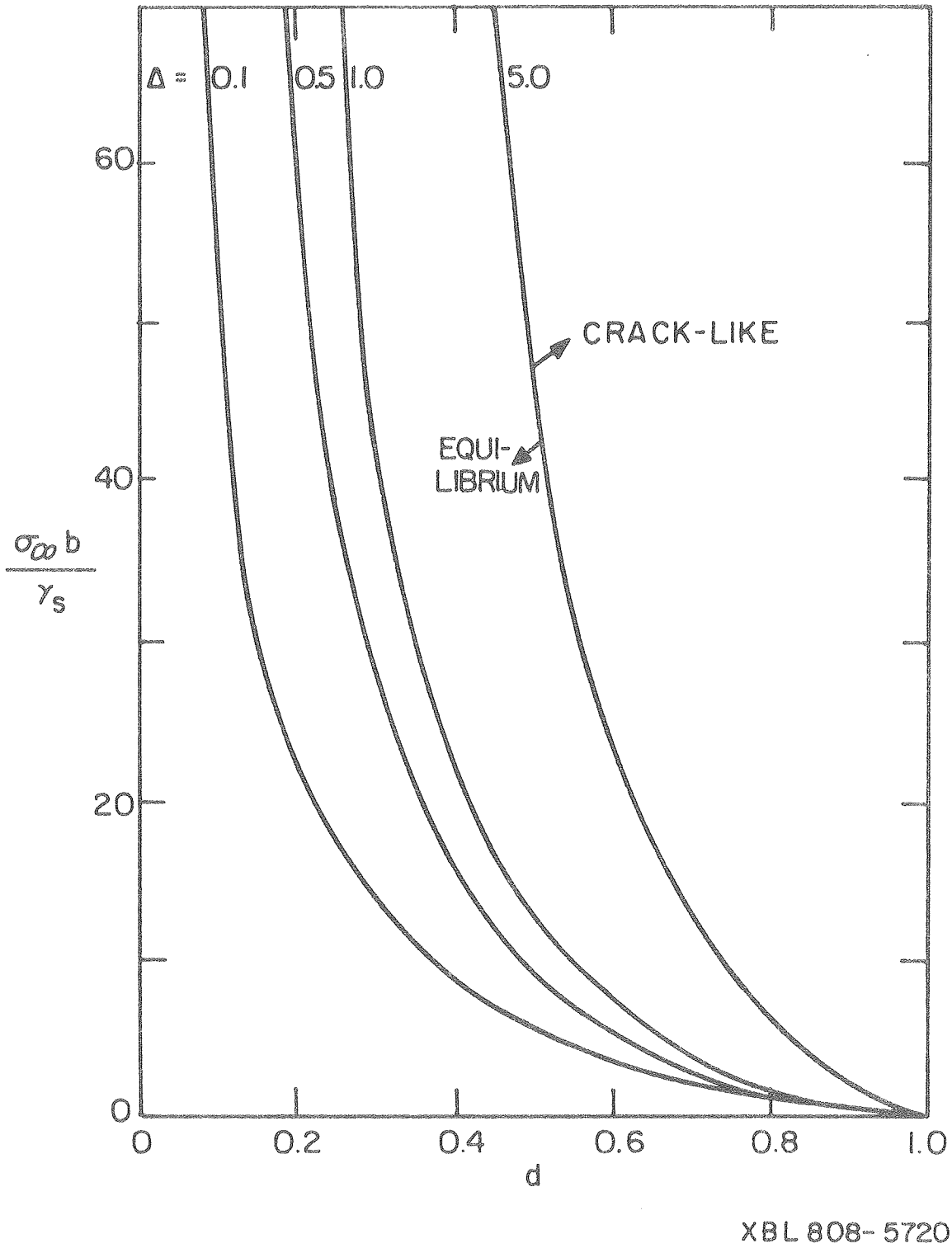
Δ =
0.1
0.5
1.0
5.0
CRACK-LIKE
EQUI-
LIBRIUM
60
40
20
0
$\frac{\sigma_\infty b}{\gamma_s}$
0
0.2
0.4
0.6
0.8
1.0
d
XBL 808-5720

Fig. 16

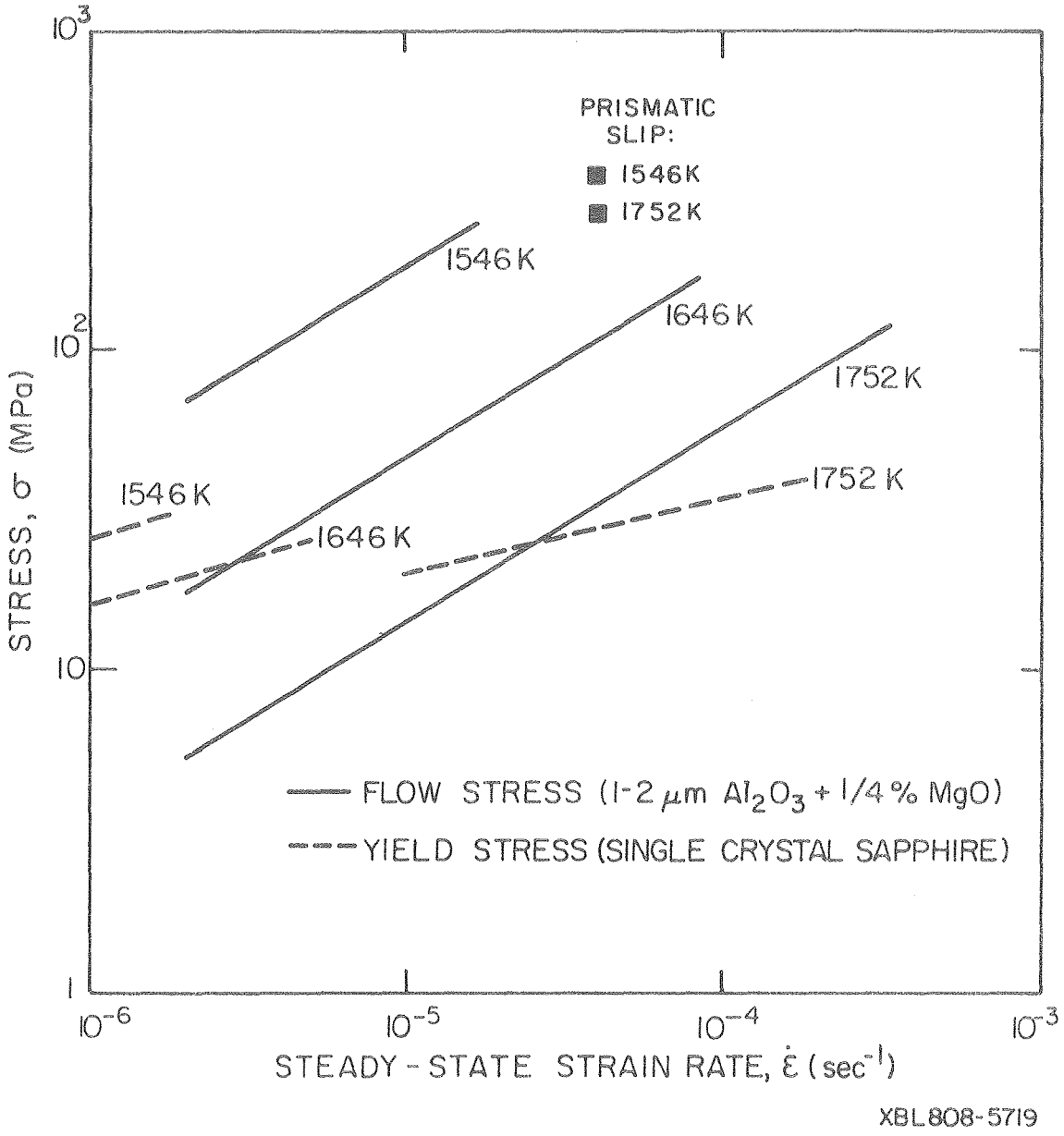
PRISMATIC SLIP:
1546K
1752K
1546K
1646K
1752K
1546K
1646K
1752K
FLOW STRESS (1-2 μm Al2O3 + 1/4% MgO)
YIELD STRESS (SINGLE CRYSTAL SAPPHIRE)
STRESS, σ (MPa)
STEADY-STATE STRAIN RATE, ε̇ (sec⁻¹)
10³
10²
10
1
10⁻⁶
10⁻⁵
10⁻⁴
10⁻³
XBL808-5719

Fig. 17